Flammability properties of intumescent vinyl acetate–ethylene copolymer emulsion including natural carbonization agent

Jinhan Lu, Luming Li, Peng Jiang, Zhilin Chen, Gaelle Fontaine, Yahui Zhang, Guoping Yu, Serge Bourbigot

Flammability Properties of Intumescent Vinyl Acetate–Ethylene Copolymer Emulsion Including Natural Carbonization Agent

Jinhan Lu [a, 1], Luming Li [b, 1], Peng Jiang [a*], Zhilin Chen [a], Gaëlle Fontaine [c*], Yahui Zhang [a], Guoping Yu [d], Serge Bourbigot [c, e*]

[a] Research Institute of Wood Industry, Chinese Academy of Forestry, Beijing 100091, P.R China

[b] School of Engineering, Zhejiang A&F University, Hangzhou 311300, P.R China

[c] Univ. Lille, CNRS, ENSCL, UMR 8207, UMET, Unité Matériaux et Transformations, F-59000 Lille, France

[d] Deqin Dingsen Quality and Technical Test Center, Huzhou 313200, P. R China

[e] Institut Universitaire de France (IUF), France

*Corresponding Author

E-mail address: jiangpeng@caf.ac.cn (P. Jiang), gaelle.fontaine@centralelille.fr (G. Fontaine), and serge.bourbigot@centralelille.fr (S. Bourbigot).

[1] These authors contributed equally to this work.

Abstract

Melamine amino trimethyl phosphate (M-AT) has been mixed with bio-based starch, chitosan, or sodium lignosulfonate (SL), and used to prepare an intumescent flame retardant (IFR) vinyl acetate-ethylene copolymer emulsion (VAE), which might be used for the formulation of adhesives, coatings, *etc*. The goal was to meet the performance requirements especially with respect to flame retardance and mechanical properties. The flammability of VAE adhesives was assessed using limiting oxygen index (LOI), UL-94 vertical burning, and cone calorimetry tests (CCT). The presence of 30 wt% of the M-AT/SL compounds (mass ratio of M-AT to SL was 3:1) in VAE polymer brought a 73 % reduction in peak of heat release rate (139.2 to 37.1 kW/m^2) in CCT. The LOI was increased to 31.5 from 20, the UL94 grade was upgraded to V-0 (sample thickness: 5 mm). The formation of bubble-shaped char layer can be promoted by polyphosphoric acid and benzenesulfonic acid along with ammonia and sulfur dioxide, which generated by the thermal decomposition of synthesized M-AT and SL during combustion of the polymer. In addition, the incorporation of 30 wt% M-AT/SL compounds in VAE matrix leaded to a 56% and 40% increasement in tensile strength and elongation at break tests, respectively compared to the pure one. This work offers a green and novel method for the production of high-performance VAE adhesives with fire resistance properties.

Keywords: Sodium lignosulfonate; intumescent flame retardant; thermal degradation; bubble-shaped.

1. Introduction

Vinyl acetate-ethylene copolymer emulsion (VAE) has been widely used in adhesives [1], coatings [2], leathers [3], constructions [4], tissues [5], and textiles [6] owing to its excellent properties for bonding, flexibility, acid/alkali resistance, creep resistance, and environmental-friendliness [7]. However, VAE is mainly composed of carbon, hydrogen, and oxygen elements, and is a kind of extremely flammable polymer, which has no rate in the UL-94 vertical burn test and the LOI value is only 19 [8-10]. High flame-spread rate, accompanied by thick-toxic smoke formation and evolution of unpleasant gas occurs during combustion of VAE polymer [11]. It is necessary to develop high-efficiency and eco-friendly flame retardants to reduce the flammability and expanded the application areas of VAE polymer.

The halogen-free intumescent flame retardants (IFRs) have attracted an increasing interest recently, due to its unique flame-retardant mode of action, low toxicity and little tendency to promote smoke formation [12]. Intumescent materials often form a foamed multicellular char layer at the surface of a degrading polymer that protects the inner material from the heat flux from the combustion zone. The presence of an expanded char layer at the polymer surface acts as a physical barrier to reduce the heat feedback to the polymer and consequent formation of volatile fuel fragments [13]. The peak heat release rate (pHRR) for combustion of an ethylene vinyl acetate elastomer containing aluminium trihydroxide and melamine phosphate was significantly lower than that for the polymer containing no additive. The pHRR was reduced from 510 to 124 kW/m^2, the LOI value was 38 vol% and a V-0 classification in UL-94 test (sample thickness: 15 mm) was achieved [14]. The presence of 15 wt% of b-cyclodextrin nanosponges, triphenyl phosphite, triethyl phosphate, ammonium polyphosphate, dibasic ammonium phosphate, or diethyl phosphoramidate blended with ethylene vinyl acetate copolymer significantly reduces the pHRR for combustion from 582 to 151 kW/m^2 with a reduction of total heat release (ca–77%) [15]. An ethylene-vinyl acetate/mica powder/organo-modified montmorillonite composite containing 23 wt% ammonium polyphosphate/zinc borate displayed a significant reduction of pHRR from 1355.6 to 179.6 kW/m^2 [16].

An IFR system generally consists three ingredients: acid source, carbonization agent, and blowing agent. Amino trimethyl phosphonic acid (ATMPA, $C_3H_{12}NO_9P_3$) is a representative scale inhibitor applied in the water healing process. The phosphate groups in the molecular structure of ATMPA provide forceful chelating ability [17]. Melamine (MEL) is used to synthesize novel flame retardants by self-assembly with organic or inorganic acids due to its ionic attractivity and propensity for π-π stacking to form multiple hydrogen bonds [18-19]. A novel MEL amino trimethyl phosphate (M-AT) was prepared from MEL and ATMPA in an aqueous solution through ionic attraction and π-π stacking self-assembly. This material can be used as the acid source and blowing agent in intumescent FR. As the carbonization agent, several natural materials such as starch, chitosan, and sodium lignosulfonate (SL) can be considered

as a substitute for pentaerythritol from petrochemicals. Starch, a typical carbohydrate widely exists in potato, wheat, corn, rice, cassava *etc.* [20]. Chitosan, a linear polysaccharide, is derived from the shells of shrimp, crabs, insects, mollusks *etc.* [21]. Sodium lignosulfonate (SL), as a low-cost and environmental-friendly additive for polymer and concrete, is prepared by a chemical modification of lignin [22]. Notably, lignin is a highly cross-linked polyphenolic polymer and the third most abundant natural polymer after cellulose and chitin. It is available as a co-product of the pulp and paper industry [23].

A novel IFR system containing M-AT and bio-based carbonization agent (starch, chitosan, or SL) has been prepared and was then introduced into a VAE matrix by blending method. The flame retardance, thermal stability, and mechanical properties of the modified VAE resins were investigated. The pyrolysis volatiles from the VAE resins were identified using thermogravimetric analysis coupled with Fourier Transform InfraRed (TGA/FTIR). Furthermore, the flame retardant mechanism in condensed phase was proposed based on the analysis of the char residues after combustion via FTIR and scanning electron microscopy (SEM).

2. Materials and Methods

2.1 Materials

Melamine (MEL), and amino trimethyl phosphonic acid (ATMPA) (50 wt%) were purchased from Sinopharm Chemical Reagent Co., Ltd. Starch soluble (AR rank, derived from corn) was purchased from Wuxi Yatai United Chemical Co., Ltd. Chitosan (Foodstuff rank, 99 wt%) was supplied by Jiangsu Gubei Biological Technology Co., Ltd. SL (AR rank, 85 %) was provided by Xian Tianmao Chemical Industry Co., Ltd. Vinyl acetate–ethylene copolymer emulsion (VAE, solid content: 55 %) supplied by GELIN HANYE Co., Ltd.

2.2 Preparation

2.2.1 Preparation of MEL-ATMPA (M-AT)

M-AT has been synthesized by MEL and ATMPA through ionic attraction and π-π stacking self-assembly [24-25]. Firstly, MEL (30 g) was dissolved in 800 mL boiling deionized water in a three-neck flask equipped with a magnetic stirrer. The pH value of the solution was then adjusted to 5-6 using 1 mol/L HCl solution with deionized water as a solvent. The obtained solution was heated to 90 °C and stirred for 30 min. After that, ATMPA (65 mL) was added into the flask and the solution was stirred for 6 h. The solution was then cooled down for 12 h and white crystal precipitated. The obtained crystals were filtered and washed with deionized water for three times. Finally, the yielding filter cake was dried at 80 °C to a constant weight, leading to M-AT (Yield = 80 %).

2.2.2 Preparation of intumescent flame retardant VAE adhesive (IFR/VAE)

The intumescent flame retardants (IFRs) were consisted of M-AT and renewable carbonization agents (starch, chitosan or SL). The preparation process of intumescent flame retardant VAE polymer (IFR/VAE) has been shown in Figure 1. The ratio of M-AT to carbonization agents was fixed at 3:1 and the formulation has been listed in Table 1. The IFR/VAE were prepared by blending 70 wt% of VAE with 30 wt% of IFRs using a high-speed mixer at a temperature of 60 °C for 30 min, and then cooled down to ambient temperature before used. The obtained IFR/VAE adhesives were injected into a curing Teflon mold (150×15×5 mm^3) and then dried in an oven at 80 °C for 12 h. The cured samples were used for the limiting oxygen index (LOI) tests, UL-94 vertical burn test, and thermal stability test. The IFR/VAE adhesives (150 g/m^2) were coated on both faces of an analysis filter paper using an adhesive roller, and then dried in an oven at 60 °C for 12 h. The processed samples with a size of 100×20×0.3 mm^3 were used for mechanical test.

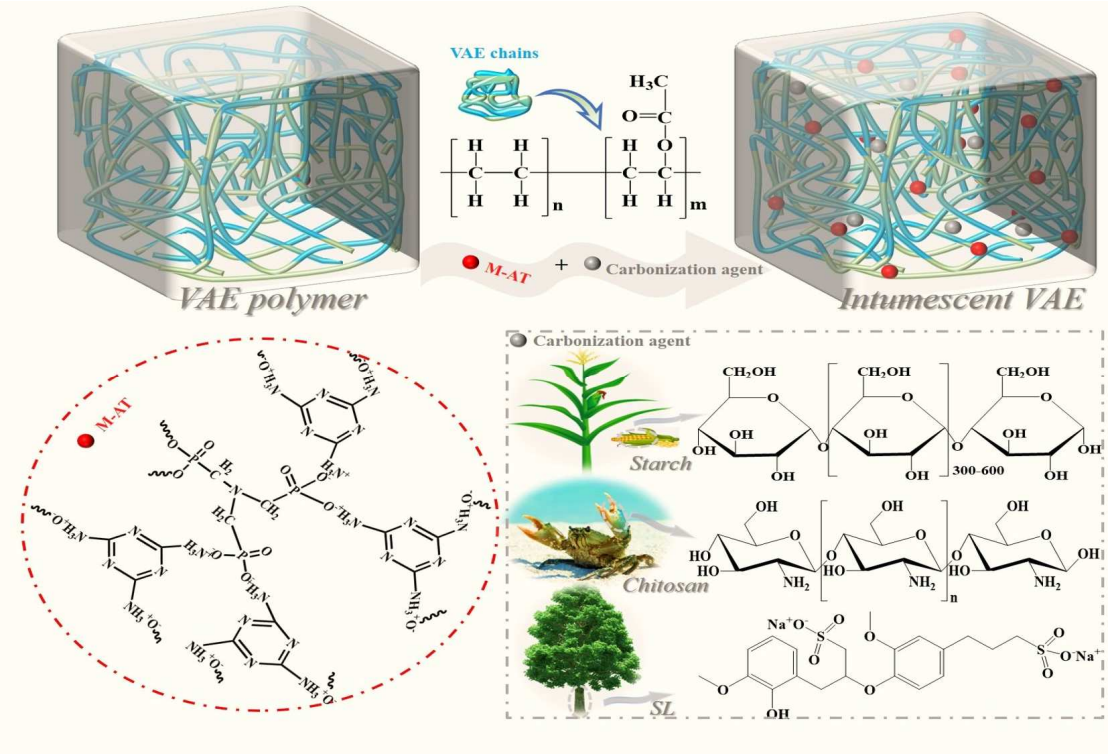

Figure 1. Preparation process of intumescent flame retardant vinyl acetate-ethylene copolymer emulsion (VAE polymer).

Table 1. Formulation of neat VAE and IFR/VAE samples.

Samples	VAE (wt.%)	M-AT (wt.%)	Starch (wt.%)	Chitosan (wt.%)	SL (wt.%)
Neat VAE	100	0	0	0	0
VAE/M-AT	70	30	0	0	0
VAE/M-AT/Starch	70	22.5	7.5	0	0
VAE/M-AT/Chitosan	70	22.5	0	7.5	0
VAE/M-AT/SL	70	22.5	0	0	7.5

2.3 Characterization

The sample particles with a sieve diameter of less than 100 mesh (150 μm) were prepared, mixed with KBr powder, pressed into the grinding dish, and placed into the Fourier-transform infrared (FTIR) spectrometer (Nicolet Nexus 670) for infrared spectroscopy analysis. X-ray photoelectron spectroscopy (XPS) measurements were performed on an ESCALAB 250 Xi spectrometer produced by Thermo Fisher Scientific company using a mono-chromated Al Kα X-ray source (hν-1486.6 eV). Thermogravimetric analysis (TGA) was conducted on a NETZSCH TG 209 instrument at a heat rate of 10 °C/min under a nitrogen atmosphere over a temperature range from 25 to 800 °C. FTIR-TGA was performed to analyze the pyrolytic gas of adhesive samples. The spectra were recorded from 600 to 4000 cm^{-1} with an accumulation of 8 scans and an optical resolution of 4 cm^{-1}. A transfer line connected the TGA instrument and the gas cell, were both heated to approximately 230 °C to prevent condensation of the decomposition products. The mass of each sample was approximately 10 mg. The calculated values of residual mass at 800 °C for VAE polymers are based on the references [26-27].

The LOI tests were performed with a JF-3 oxygen index apparatus (Jiangning Analysis Instrument Company, China) on the basis of ASTM D 2863-17 with a sample size of 100 × 10 × 5 mm^3. UL-94 vertical burning tests were performed on a Jiangning CZF-5 apparatus (Jiangning Analysis Instrument Company, China) with a sample size of 125 × 13 × 5 mm^3. The digital pictures and weight for samples were recorded before and after the thermal treatment using a muffle furnace under 500 °C for 3 minutes. The weight of each sample was 0.5 g.

The IFR/VAE adhesives (1500 g/m^2) were coated on the surface of steel (100×100×3 mm^3) for three times, and each time needed 500 g/m^2 in a week for curing. The coated steel samples were used for combustion behavior test. The combustion behavior was analyzed using a cone calorimeter (Fire Testing Technology Ltd., East Grinsted, U.K.) according to ASTM E1354-17 under a heat flux of 50 kW/m^2. During the cone calorimeter test (CCT), the heat release rate (HRR) was measured as a function of time on the basis of oxygen consumption principle; and time to ignition (TTI), total heat release (THR), peak of HRR (pHRR), peak of CO yield (pCOY), and total smoke production (TSP) were obtained after CCT. Besides, some essential parameters like the maximum average heat rate emission (MAHRE, defined as maximum value of the cumulative heat emission divided by time), the fire growth rate (FIGRA, defined as the maximum value of HRR(t) divided by time), and the fire performance index (FPI, defined as a value of TTI divided by pHRR) could be calculated according to the data obtained by CCT [28-29].

Field-emission scanning electron microscopy (FE-SEM) (Model SU8010, Hitachi) combined with an energy-dispersive X-ray (EDX) detector was used to characterize the morphology of the samples. The laser Raman spectroscopy (LRS) measurements were performed on a Raman micro-spectrometer (Renishaw in Via type) with

scanning region was ranged from 50 to 4000 cm^{-1}. The excitation by a 514.5 nm helium-neon laser line focused a micrometer spot on the sample surface. The mechanical properties of samples were analyzed on a CMT4104 tensile testing machine (SANS Company, China) according to ASTM test methods (D-638). The samples were tested with a speed of 5 mm/min.

3 Results and discussion

3.1 Intumescent behavior

Figure 2a shows the schematic diagram for the synthesis of M-AT. The XPS spectra is applied to confirm the self-assembly behavior of MEL and ATMPA and have been shown in Figure 2b and 2c. The typical peaks of MEL remained in M-AT, and the new peaks at 133.1 and 191.1 eV corresponding to P_{2p} and P_{2s} of ATMPA respectively, have been observed in Figure 2b. Furthermore, the peak intensity of O_{1s} in M-AT is significantly higher than in MEL, which can be attributed to the self-assembly of MEL and ATMPA. The peaks at 398.8 and 399.5 eV corresponded to C-N=C and -NH- from MEL [24]. Notably, the peak at 401.0 eV assigned to NH_3^+ group, which demonstrates the successful self-assembly between MEL and ATMPA. A smooth surface morphology of MEL is clearly visible and shown in Figure 2d. However, the morphology of M-AT is significantly transformed after the self-assembly with ATMPA and a plate-like π-π stacking of triazine rings structure of MEL-AT can be seen in Figure 2e.

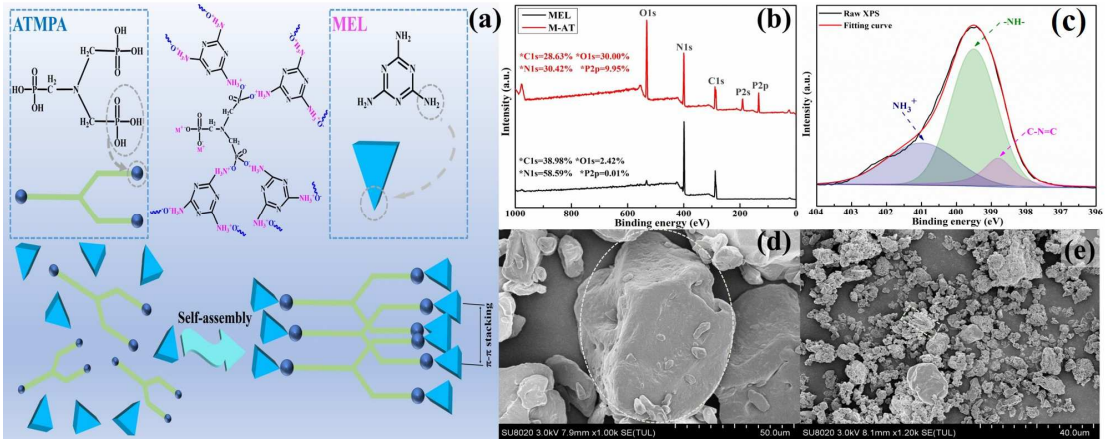

Figure 2. a) Preparation process of M-AT; b) XPS spectra of MEL and M-AT; c) N_{1s} fitted peaks of M-AT; d) and e) SEM images of MEL and M-AT.

Figure 3a shows the TGA curves of M-AT, starch, chitosan, and SL. The amounts of char residues at 800 °C for M-AT, starch, chitosan, and SL are 44.0 %, 17.1 %, 22.6 %, and 42.8 % respectively, which indicates that M-AT and SL have a better charring ability than starch and chitosan. Figure 3b and 3c show the charring results of M-AT, M-AT/Starch, M-AT/Chitosan, and M-AT/SL samples after thermal treatment using a muffle furnace. The expansion percentage of M-AT/Starch, M-AT/Chitosan, and M-AT/SL is 275 %, 283 %, and 250 % relative to the M-AT sample, indicating a

similar increase ability on the expansion height shown in Figure 3b. The mass losses of M-AT, M-AT/Starch, M-AT/Chitosan, and M-AT/SL samples after thermal treatment in a muffle furnace under 500 °C for 3 minutes are 46.3 %, 52.9 %, 58.9 %, and 69.1 %, respectively, which indicates that the natural carbonization agents significantly enhance the charring ability of M-AT.

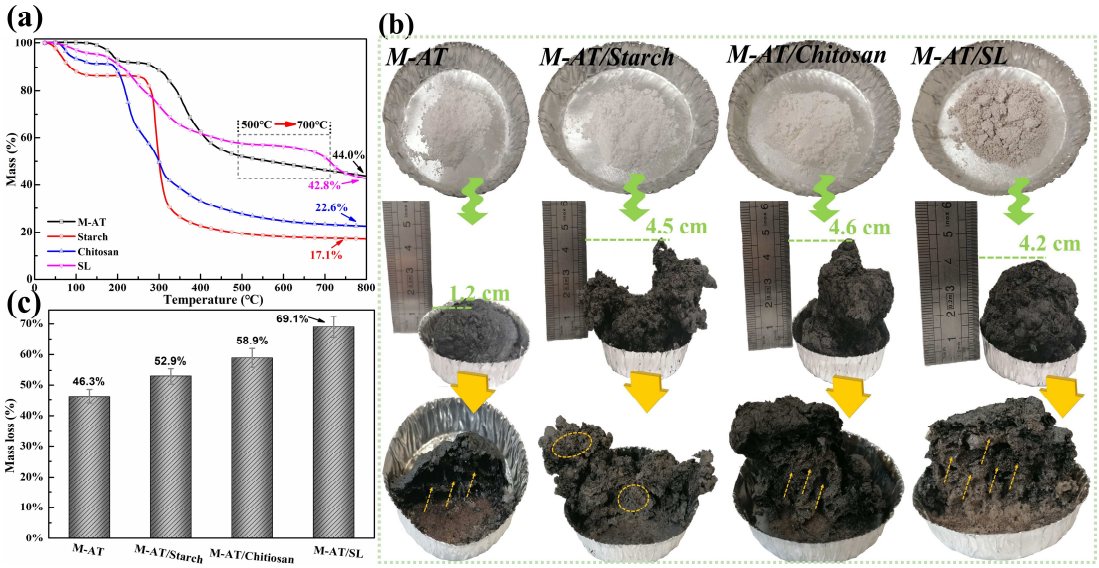

Figure 3. a) TGA results of M-AT, starch, chitosan, and SL under nitrogen atmosphere at a heat rate of 10 °C/min; b) Digital pictures of samples M-AT, M-AT/Starch, M-AT/Chitosan, and M-AT/SL before and after thermal treatment in a muffle furnace under 500 °C for 3 minutes; c) Mass loss samples M-AT, M-AT/Starch, M-AT/Chitosan, and M-AT/SL after thermal treatment in a muffle furnace under 500 °C for 3 minutes.

3.2 Thermal behavior

The TGA curves of neat VAE and IFR/VAE samples under N_2 are shown in Figure 4 (a, b), and key data are listed in Table 2. Figure 4a shows three decomposition steps for neat VAE sample: decomposition of vinyl acetate with the production of volatilized acetic acid occurred from 240 to 360 °C, oxidative degradation of polyethylene chains occurred from 380 to 480 °C [30-32], and a char residue value of 2.3 % at 800 °C is obtained. The amounts of char residues for sample VAE/M-AT increases to 14.0 % compared to the same value of polymer containing no additive. Notably, samples VAE/M-AT/Starch (15.9 %), VAE/M-AT/Chitosan (17.9 %), and VAE/M-AT/SL (20.6 %) exhibit a higher amount of char residues at 800 °C compared to sample VAE/M-AT, indicating a good thermal stability of natural carbonization agents (*i.e.*, starch, chitosan, or SL) containing IFRs. The enhanced thermal stability of VAE polymer loading intumescent materials relative to the polymer containing no additive, which is ascribed to the degradation of the M-AT to generate polyphosphoric acids, water, and ammonia under heat, thus protecting the inner materials from heat [33-34]. In addition, the experimental char residues for samples VAE/M-AT/Starch, VAE/M-AT/Chitosan, and VAE/M-AT/SL are higher

than calculated values listed in Table 2, which can be attributed to the good charring capability of natural carbonization agents (*i.e.*, starch, or chitosan, especially, SL) for M-AT as shown from the result of thermal treatment in Figure 3c. Moreover, SL had a better charring ability than starch and chitosan. The excellent thermal stability of SL could be ascribed to the benzene ring structure in the lignin chemical structure. Additionally, benzenesulfonic acids along with the release of sulfur dioxide were generated from the degradation of SL under heat, which was beneficial for the formation of bubble-shaped char layers. Furthermore, sample VAE/M-AT/SL exhibits the highest reduction of maximum mass loss rate values compared to starch and chitosan containing intumescent flame retardant samples, which suggests an excellent effect on suppressing the thermal decomposition of the VAE matrix at high temperatures.

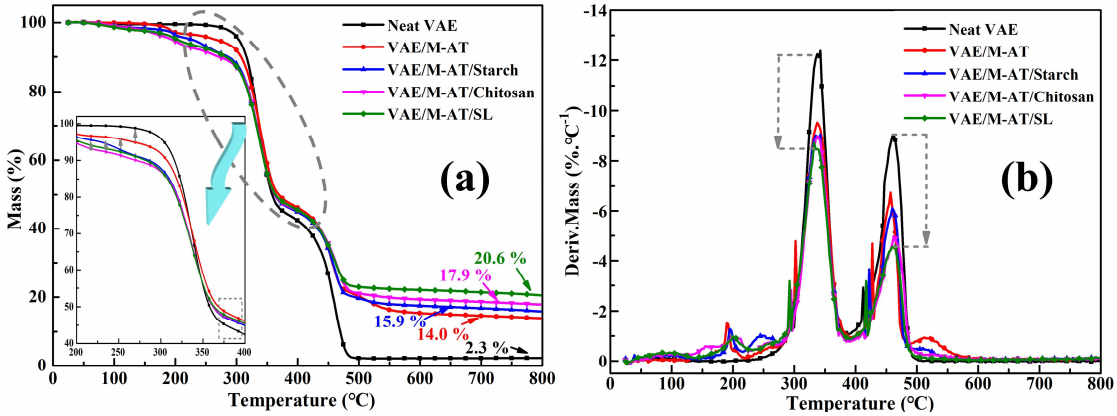

Figure 4. a) TGA and b) derivative thermogravimetry (DTG) of the neat VAE and IFR/VAE samples under N_2 atmosphere at a heat rate of 10 °C/min.

Table 2. Essential data of samples neat VAE and IFR/VAE in TGA under nitrogen atmosphere.

Samples	$T_{max\ 1}$ (°C)	$T_{-5wt\%}$ (°C)	$T_{max\ 2}$ (°C)	$T_{max\ 3}$ (°C)	Char residue (%) at 800 °C	
					Experimental	Calculated
Neat VAE	-	305	341	461	2.3	-
VAE/M-AT	190	265	340	457	14.0	14.8
VAE/M-AT/Starch	197	227	340	461	15.9	12.8
VAE/M-AT/Chitosan	200	195	338	462	17.9	13.2
VAE/M-AT/SL	200	205	333	464	20.6	14.7

3.3 Fire behavior

3.3.1 LOI and UL-94 test

The LOI values and UL-94 (sample thickness: 5 mm) rating of neat VAE and flame retarded VAE have been listed in Table 3. The neat VAE sample has no rate in the UL-94 vertical burn test together with dripping behavior and the LOI value is only 20 vol %. The LOI value increases to 29 vol % with the incorporation of 30 wt% M-AT (VAE/M-AT). In addition, the LOI values of samples VAE/M-AT/Starch, VAE/M-

AT/Chitosan, and VAE/M-AT/SL are enhanced to 28 vol %, 30 vol % and 32 vol % respectively, which represents an increasement of 40, 50 and 60 % respectively compared to neat VAE sample, and V-0 rating has been achieved for all three flame retardant samples. The SL-containing intumescent VAE polymer exhibits the maximal increasement of the LOI value.

Table 3. LOI and UL-94 test results of neat VAE and IFR/VAE samples.

Sample	LOI	△LOI	UL-94 (thickness: 5 mm)		
			Dripping	Rating	t1/t2 (s)
Neat VAE	20±0.2	-	Y	N	t1+t2>60
VAE/M-AT	29±0.3	+9	N	V-0	0/0
VAE/M-AT/Starch	28±0.3	+8	N	V-0	0/0
VAE/M-AT/Chitosan	30±0.1	+10	N	V-0	0/0
VAE/M-AT/SL	32±0.2	+12	N	V-0	0/0

3.3.2 Cone calorimeter test

The fire performance of neat VAE and IFR/VAE samples has been further analyzed using CCT. HRR and THR curves have been obtained and shown in Figure 5a and 5b. The HRR curves of neat VAE and IFR/VAE samples display a "double-peak" behavior shown in Figure 5a and 5b, which is attributed to a representative phenomenon in thermally thick charring samples: an initial increase in HRR occurs until an efficient char layer is formed, as the char layer thickens, this results in a decrease in HRR; and the continuously exposed to the flame caused the second peak HRR [35].

The double-peak in HRR curves of neat VAE with values of 267 and 139 kW/m^2 occurred at 90 and 165 s, respectively. The incorporation of intumescent flame retardant significantly reduces the HRR values of VAE adhesives. The 1st peak-HRR (pHRR 1) of VAE/M-AT/Starch, VAE/M-AT/Chitosan, and VAE/M-AT/SL samples exhibit a reduction of 27 %, 33 %, and 48 % respectively compared to the neat VAE sample. The 2nd peak-HRR (pHRR 2) of VAE/M-AT/Starch, VAE/M-AT/Chitosan, and VAE/M-AT/SL samples also display a great decrease of 60 %, 60 %, and 73 %, respectively, relative to the neat VAE sample. Moreover, the incorporation of IFRs substantially reduces the THR values from 28 MJ of neat VAE to 17, 19, and 14 MJ of VAE/M-AT/Starch, VAE/M-AT/Chitosan, and VAE/M-AT/SL, respectively. The SL-containing intumescent VAE polymer exhibits a far superior effect by suppressing the heat release during combustion process which is better than the starch and chitosan containing samples.

The key cone calorimetry data of samples neat VAE and IFR/VAE are listed in Table 4. The MAHRE values of VAE/M-AT/Starch, VAE/M-AT/Chitosan, and VAE/M-AT/SL samples represent a reduction of 30 %, 18 %, and 40 % respectively, relative to the neat VAE sample. The FIGRA and FPI have been used to evaluate the hazard of developing fires. The lower FIGRA indicates lower fire risk while the higher FPI

value indicates higher fire safety rank. Samples VAE/M-AT/Starch (3.3 kW/m^2.s) and VAE/M-AT/SL (2.3 kW/m^2.s) show a lower FIGRA than sample neat VAE (3.6 kW/m^2.s). In addition, samples VAE/M-AT/Chitosan (0.4 m^2.s/kW) and VAE/M-AT/SL (0.5 m^2.s/kW) represent a higher FPI than neat VAE (0.3 m^2.s/kW). This indicates that the fire resistance of VAE polymers has been significantly enhanced by incorporating the IFRs composed of M-AT and SL compound.

Besides, the pCOY of samples VAE/M-AT/Starch, VAE/M-AT/Chitosan, and VAE/M-AT/SL represent a substantial reduction of 85 %, 77 %, and 75 %, respectively, compared to the neat VAE sample. The TSP values from 2.9 m^2 of neat VAE sample is reduced to 2.1, 2.2 and 2.4 m^2 of VAE/M-AT/Starch, VAE/M-AT/Chitosan, and VAE/M-AT/SL samples, respectively. It is concluded that the introduction of M-AT and SL compound decreased the release of toxic gas (*i.e.,* CO) and smoke.

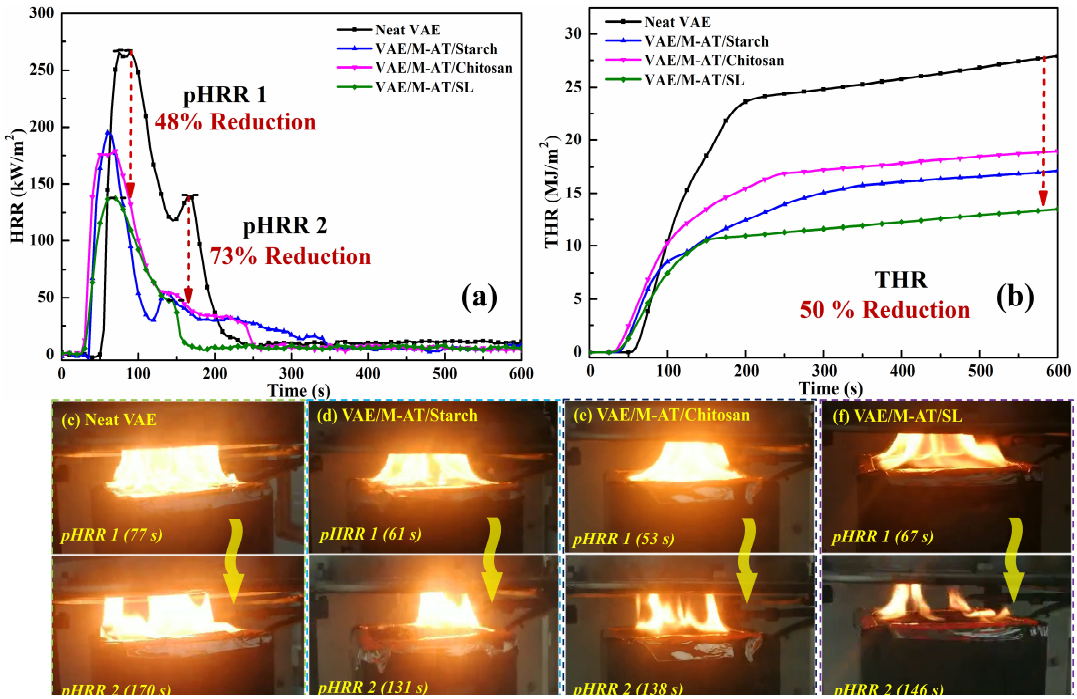

Figure 5. a) HRR and b) THR curves of the neat VAE and IFR/VAE samples during CCT at a flux of 50 kW/m^2, digital pictures at pHRR 1 and pHRR 2 of neat VAE (d), VAE/M-AT/Starch (d), VAE/M-AT/Chitosan (e) and VAE/M-AT/SL (f) during CCT.

Table 4. Cone calorimetry data of the neat VAE and IFR/VAE samples.

Samples	pHRR 1 (kW/m^2)	pHRR 2 (kW/m^2)	THR (MJ/m^2)	MAHRE (kW/m^2)	FIGRA (kW/m^2.s)	FPI (m^2.s/ kW)	pCOY (kg/kg)	TSP (m^2)
Neat VAE	267	139	28	125	3.6	0.3	2122	2.9
VAE/M-AT/Starch	195 (-27%)	56 (-60%)	17 (-39%)	87 (-30%)	3.3	0.3	309 (-85%)	2.1
VAE/M-AT/Chitosan	179 (-33%)	55 (-60%)	19 (-32%)	102 (-18%)	3.7	0.4	492 (-77%)	2.2
VAE/M-AT/SL	138 (-48%)	37 (-73%)	14 (-50%)	75 (-40%)	2.3	0.5	536 (-75%)	2.4

3.4 Mode action of IFR/VAE

3.4.1 Gas phase analysis

In order to explore the gaseous-phase behavior of IFRs, TGA-FTIR experiments were used to identify the pyrolysis volatiles of neat VAE and IFR/VAE samples. The 3D TGA-FTIR graphs shown in Figure S1 indicated that the real-time absorbance of pyrolysis volatiles of the neat VAE and IFR/VAE samples as a function of temperature. Overall, the incorporation of 30 wt% of IFRs significantly reduces the gaseous-products except carbon dioxide, as revealed through the decreased absorbance intensity, which indicating the thermal degradation of VAE polymer can be suppressed by the IFRs. Figure 6a shows the FTIR spectra of pyrolysis volatiles for the thermal decomposition of the neat VAE sample at different temperature. The peaks of water (H_2O) (3577 cm^{-1}), hydrocarbons (3056 to 2840 cm^{-1}, 1448 cm^{-1}, and 1384 cm^{-1}), carbonyl (C=O) (1795 and 1776 cm^{-1}), C-O (1178 cm^{-1}), and hydroxyl (O-H) deformation (651 and 684 cm^{-1}) are detected [34-35]. Figure 6b shows the cumulative FTIR spectra of the degradation productions for neat VAE and IFR/VAE samples. In comparison with the neat VAE, the addition of IFRs noticeably reduces the absorbance intensity of H_2O, C-H, C=O, and C-O. Besides, the characteristic peaks of ammonia (NH_3) (966 and 931 cm^{-1}) and carbon dioxide (CO_2) (2358 cm^{-1}) are identified [38], which plays an essential role in promoting the expansion of the molten char. Meanwhile, the FTIR spectra of decomposed gaseous-products for neat VAE and IFR/VAEs at the maximum degradation stage according to TGA results in Table 4 ($T_{max\ 2}$ and $T_{max\ 3}$) are extracted to examine the pyrolysis process in Figure 6c and 6d. It is indicated that weak vibration peak of aliphatic substituted phenols at 3739 cm^{-1} are detected at the $T_{max\ 1}$ for IFR/VAEs while disappear at the $T_{max\ 2,}$ and the absorbance intensity of H_2O, C-H, C=O, C-O of IFR/VAEs is significantly decreased compared to neat VAE.

The maximum volatiles release intensity of VAE polymers significantly decreased after incorporating the IFRs and shown in Figure 7a, which is in compliance with the DTG results shown in Figure 5b. Figure 7b- f shows that the CO_2, NH_3, C-H, C=O, and C-O gas volatiles absorption intensity of neat VAE and IFR/VAEs respectively. The absorption intensity of the diluted gases, *i.e.*, CO_2 and NH_3, has been increased for intumescent VAE polymer relative to the pure one, which can be attributed to the formation of bubble-shaped charring layers. In addition, the absorption intensity of pyrolysis volatiles of IFR/VAEs, *i.e.*, C-H, C=O, and C-O, is significantly reduced, which indicated that less gas was released in the gas phase and more char residues were left.

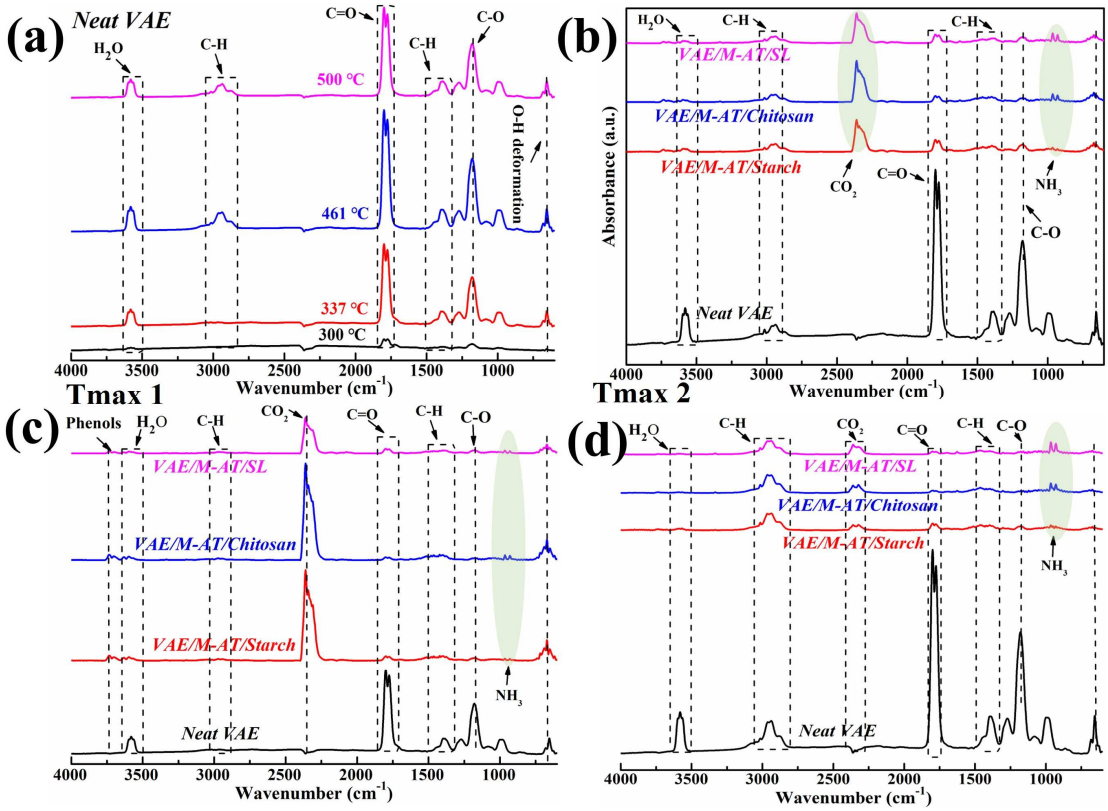

Figure 6. a) FTIR spectra of neat VAE at different temperatures, b) Cumulative FTIR spectra of the degradation productions for neat VAE and IFR/VAE samples, c) and d) FTIR spectra of neat VAE and IFR/VAE samples at two maximum thermal degradation stages in Table 4.

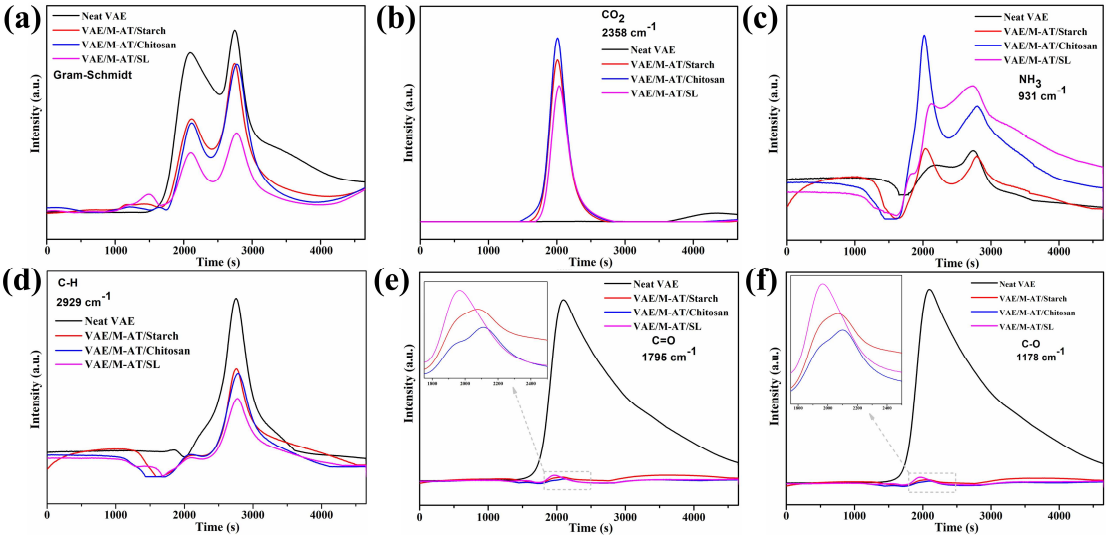

Figure 7. Absorption pyrolysis as a function of time for neat VAE and IFR/VAEs: (a) Gram-Schmidt, (b) CO_2, (c) NH_3, (d) C-H, (e) C=O, and (f) C-O.

3.4.2 Condensed phase analysis

3.4.2.1 Morphology of char residue

Neat VAE samples completely burned after the cone test, while abundant char residues of IFR/VAEs were collected after cone test. Figure 8 shows the digital photographs, SEM images and EDX spectra of char residues for IFR/VAE samples after cone test. Abundant blocky and visible-dark char residues are observed for VAE/M-AT/Starch and VAE/M-AT/Chitosan samples, while the sample VAE/M-AT/SL exhibits a more continuous, smooth, and dense char residue in the digital photographs after CCT. The surface morphology of char residues for starch containing sample exits some visible holes and the bubble-shape structure features are not obvious in SEM images after combustion. As for the chitosan containing sample, little bit bulky bubble assemblies are attached on the surface of char residues in SEM images. Differently, numerous of bubbles with viscous feature adhered tightly on the surficial char layer for the SL containing sample in SEM images after combustion. Meanwhile, the EDX results show that the VAE/M-AT/SL sample exhibits the highest P content (17.63 %) of bubble structure on the surface char layer compare to samples VAE/M-AT/Starch (16.09 %) and VAE/M-AT/Chitosan (9.41%). Furthermore, the high oxygen and phosphorous percentages in the char obtained from VAE/M-AT/SL indicated that a tough phospho-carbonaceous closed cell char has been formed.

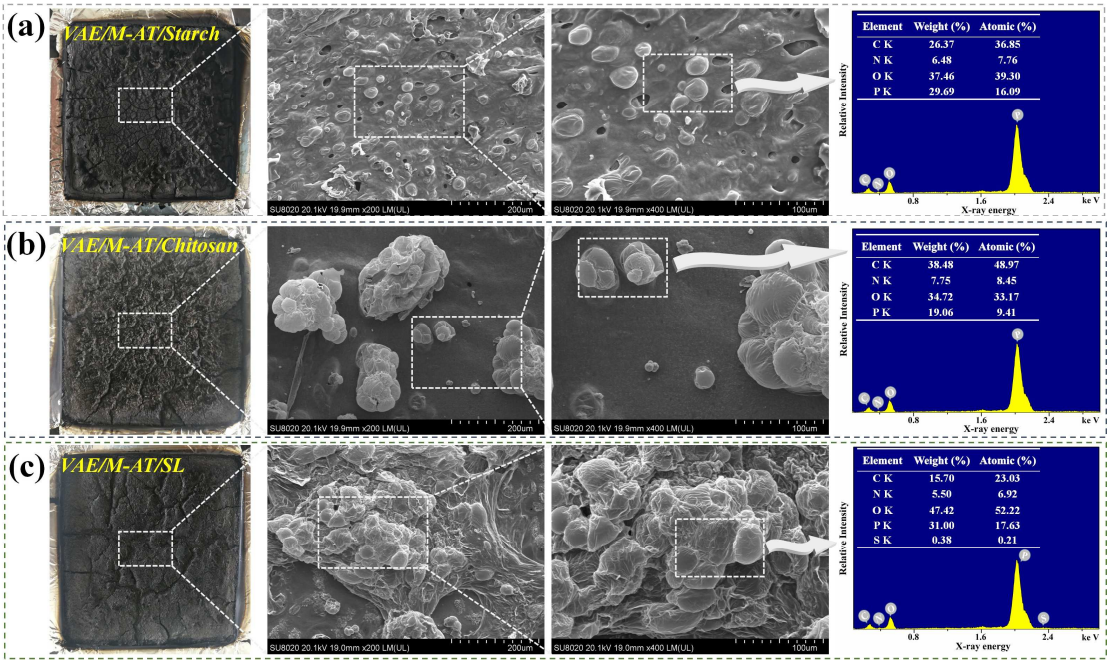

Figure 8. Digital photographs, SEM images and EDX spectra of char residues after cone test for samples VAE/M-AT/Starch (a), VAE/M-AT/Chitosan (b), and VAE/M-AT/SL (c).

3.4.2.2 LRS analysis of char residue

The LRS spectra of char residues for samples VAE/M-AT/Starch, VAE/M-AT/Chitosan, and VAE/M-AT/SL are shown in Figure 9. The D band (1355 cm^{-1}) attributed to the vibration of carbon atoms in the amorphous sphere, and the G band (1594 cm^{-1}) ascribed to the sp^2 in-plane stretching vibration of carbon atoms in the

crystalline graphite state. The degree of graphitization of the char residues could be calculated by an area ratio (R) of the D to G bands [39]. The lower value of R represents a higher graphitization degree. The char residues for VAE/M-AT/SL sample shows the lowest value of R (2.51) relative to samples VAE/M-AT/Starch (3.01) and VAE/M-AT/Chitosan (2.77), indicating the highest graphitization degree of the char residues for VAE adhesives based on M-AT/SL.

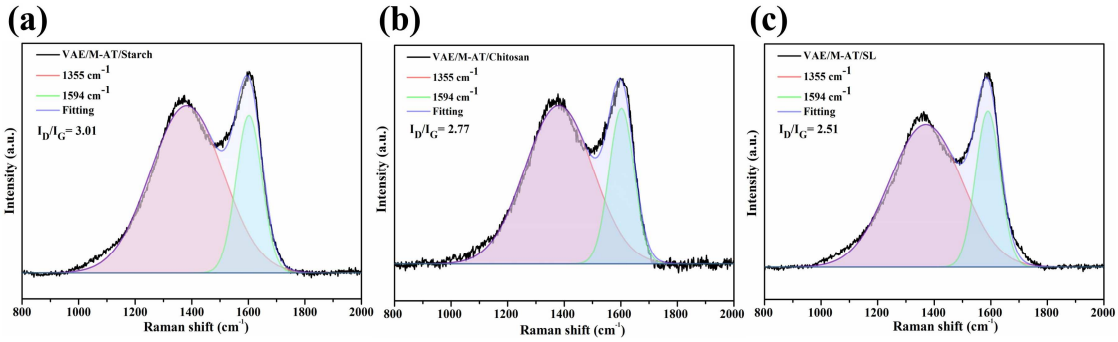

Figure 9. LRS spectra of char residues after cone test for samples VAE/M-AT/Starch (a), VAE/M-AT/Chitosan (b), and VAE/M-AT/SL (c).

3.5 Evolution of intumescent char layer

The thermal treatment using the muffle furnace at different temperatures was carried out for VAE/M-AT/SL sample to investigate the flame retardant mechanism. The treating time is 30s at each temperature, and the sample size is 20 × 20× 2 mm^3. The digital pictures, FTIR spectra, and SEM images of VAE/M-AT/SL sample after treated in a muffle furnace at different temperature have been shown in Figure 10 and Figure 11.

The VAE/M-AT/SL sample achieves the highest expansion height (1.2 cm) at a temperature of 450 °C, which is six times higher than that of the initial thickness. It is noticeable that the expansion height was reduced from 1.2 cm at 450 °C to 0.5 cm at 600 °C. The char residues were analyzed by FTIR, the characteristic peaks of C-H stretching vibration (2924 and 2894 cm^{-1}), C=O stretching vibration (1738 cm^{-1}), C-H deformation vibration (1374 cm^{-1}) for VAE are detected [40]. The peak of 1502 cm^{-1} corresponding to NH_3^+ groups is observed above 250 °C, while it disappears when the temperature rising to 400 °C, indicating the degradation of -NH_3^+-O- in M-AT [41]. The peak of P-O-P located at 1233 cm^{-1} appears above 250 °C, which can be ascribed to the formation of cross-linked polyphosphoric acids. Meanwhile, the peak of P-N-C at 1018 cm^{-1} is detected above 250 °C, which indicated that the decomposed products of ATMPA and MEL (mainly melem and melon) contribute to the formation of the cross-linking char [42-44]. Moreover, the absorbance intensity of S=O peak at 1152 cm^{-1} decreases above 300 °C, which is ascribed to the degradation of benzenesulfonic acids and the releases of SO_2 [41, 45].

As shown, the physical shape of IFR adhesive was transformed with blocky, shrinking, and lumpy features from 250 °C to 350 °C. Afterward, the bubble-shape charring layer starts to be formed on the surface from 400 °C to 500 °C, which is consistent with expansion height shown in Figure 10a. Over 500 °C, the bubble-shape structure layer was concentrated on the surface of char residues. Generally, the char residues of VAE/M-AP/SL sample underwent the process of crack, shrink, melt, bubbling and enrichment.

The flame retardant mechanism of VAE loaded M-AP/SL samples can be concluded as follows: a) the blowing effect under heat in the gas phase attribute to the released gases, such as ammonia, water vapor, carbon dioxide, and sulfur dioxide (shown in Figure 6 and Figure 10). b) the P-O-P, P-N-C, and S=O chemical structures were detected in the viscous and bubble-shaped char residues and led to the formation of a thermally stable phosphor-carbonaceous structure in the solid phase (shown in Figure 8, 10b and Figure 11) and reduce the heat conductivity and heat transfer during combustion of VAE polymer.

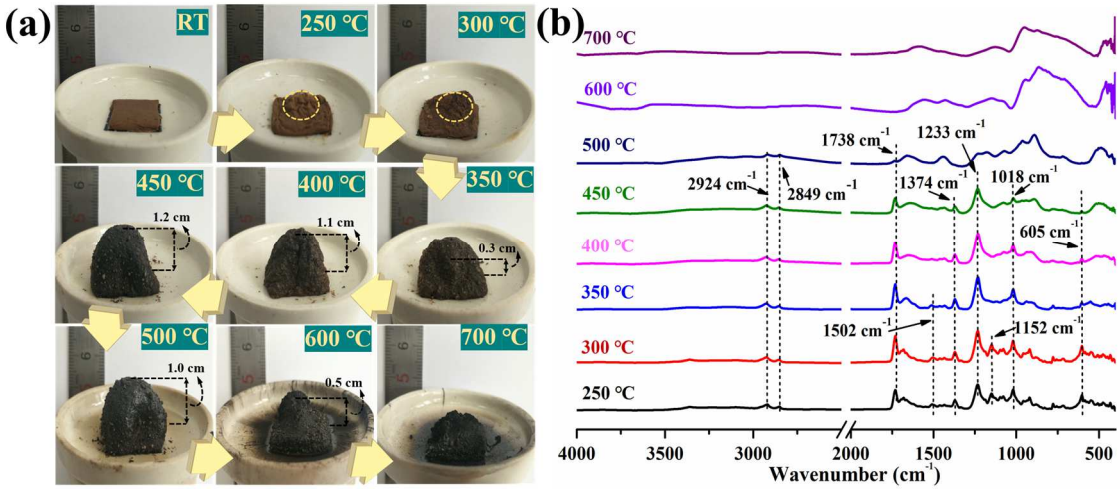

Figure 10. a) Digital pictures and b) FTIR analysis of char residues for VAE/M-AT/SL under a muffle furnace at different temperature.

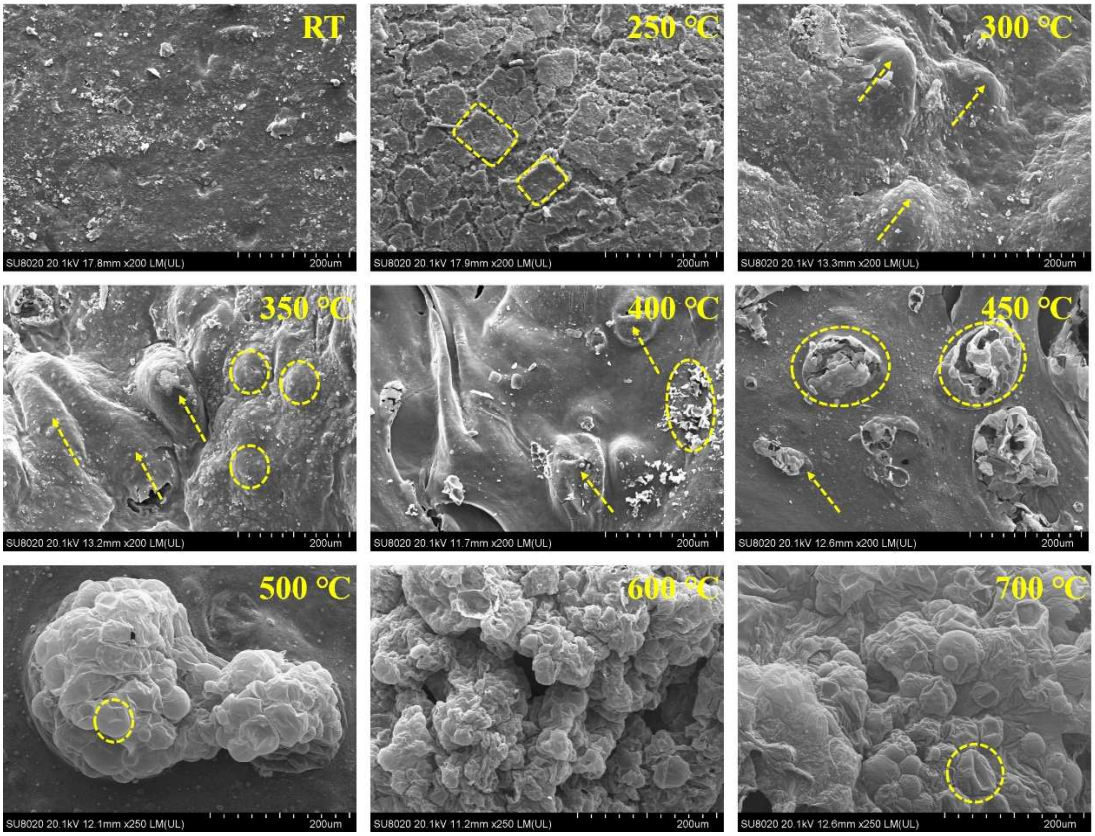

Figure 11. SEM images of char residues for VAE/M-AT/SL under a muffle furnace at different temperature.

3.6 Mechanical properties

Figure 12 shows the mechanical properties of neat VAE and IFR/VAE samples. Neat VAE shows a tensile strength of 12.4 MPa and an elongation at break of 6.1 %. However, the tensile strength of VAE/M-AT and VAE/M-AT/Starch samples represent a reduction of 11 % and 15 % respectively compared to that of the neat VAE, which can be due to the adverse effect of M-AT and M-AT/Starch on curing process for VAE adhesives [25]. Notably, an increase of tensile strength for VAE/M-AT/Chitosan (5 %) and VAE/M-AT/SL (56 %) samples are achieved compared to that of the neat VAE, which may be ascribed to the natural bonding performance of chitosan and SL [46-48]. Typically, the tensile strength of VAE/M-AT/SL sample increased significantly compared to that of the neat one by the incorporation of M-AT/SL compound. Figure S2 presents good compatibility between the incorporated M-AT/SL compound with VAE adhesive matrix. Furthermore, the lignosulfonates exhibit a higher degree of sulfonation, a lower surface tension, and the OH group in lignin contributed to improved bond strength [49-50]. As a conclusion, the VAE/M-AT/SL sample presents an excellent mechanical property.

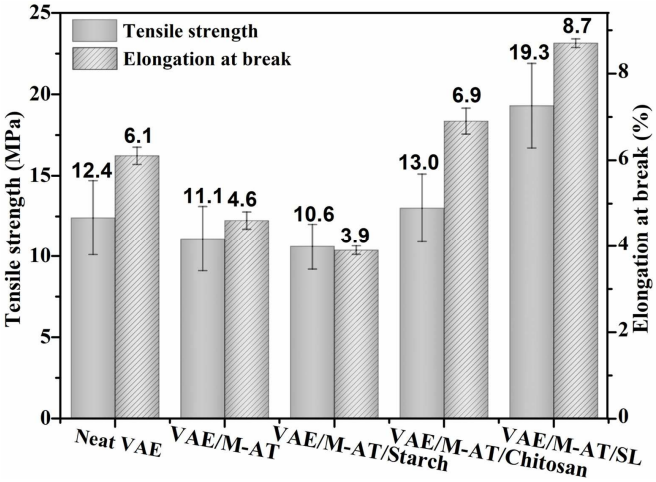

Figure 12. Mechanical properties of the neat VAE and IFR/VAE samples.

4. Conclusions

An innovative and efficient intumescent flame retardant formulation was prepared incorporating synthesized nitrogen-phosphorus compounds and natural SL to enhance the fire resistance, thermal stability, and mechanical properties of VAE adhesives. The LOI value of this flame retarded VAE polymer was increased to 31.5% with V-0 classification at UL-94 (sample thickness: 5 mm) by the presence of 30 wt% M-AT/SL, and TGA results showed that the mass of char residue at 800 °C was increased to 20.6% from 2.3% for neat VAE. In addition, the 1st and 2nd pHRR of VAE/M-AT/SL sample exhibited a reduction of 48.3% and 73.3% respectively evaluated by CCT, compared to the neat VAE. The tensile strength of VAE polymers resulted in an increase of 56% by the incorporation of M-AT/SL. We optimized the bio-based carbonization agent in IFRs for the high value-added application of VAE polymers, and this green, fire resistant, and strong adhesive expected to widely used in construction, leathers, textile areas, *etc*.

5. Acknowledgments

The authors wish to thank National Forestry public welfare industry research project (CAFYBB2021ZX001), Scientific Research Project of Zhejiang Provincial Market Supervision Administration (20210149), and the China Scholarship Council (CSC: 202003270033) for their financial contributions.

7. Declaration of Competing Interest

The authors declare no competing financial interests.

8. References

[1] Abdel W.W., Fahmy A., Kamoun E.A. A new route for synthesis of polyurethane vinyl acetate acrylate emulsions as binders for pigment printing of cotton fabrics. Egypt. Jour. Chem. 63 (2020) 1063–1073.

[2] Bompadre F., Scheffler C., Utech T. Polymeric coatings for AR-glass fibers in cement-based matrices: effect of nano-clay on the fiber-matrix interaction. Appl. Sci. 11 (2021) 5484.

[3] Abdikarimov M.N., Turgumbayeva R.K., Sartayev D.T. Investigation of pyrolysis and flammability process of vinyl acetate copolymer paints. Jour. Chem. Tech. Meta. 54 (2019) 48–54.

[4] Tarannum N., Pooja K., Khan R. Preparation and applications of hydrophobic multicomponent based re-dispersible polymer powder: a review. Cons. Build. Mate. 247 (2020) 118579.

[5] Wang Y., Wang X., Xie Y. Functional nanomaterials through esterification of cellulose: a review of chemistry and application. Cellulose. 25 (2018) 3703–3731.

[6] Abdollahi M., Bigdeli P. Reverse iodine transfer radical copolymerization of vinyl acetate and vinyl benzoate: a kinetic study. Poly. Bull. 75 (2018) 1823–1841.

[7] Zhang N., Wang S., Gibril M.E. The copolymer of polyvinyl acetate containing lignin-vinyl acetate monomer: synthesis and characterization. Euro. Poly. Jour. 123 (2020) 109411.

[8] Shi G., Huang C., Cao X. Triple shape memory effect of ethylene-vinyl acetate copolymer/poly (propylene carbonate) blends with broad composite ratios and phase morphologies. Polymer. 231 (2021) 124144.

[9] Cheng L., Liu S., Yu W. Recyclable ethylene-vinyl acetate copolymer vitrimer foams. Polymer. 222 (2021) 123662.

[10] Hong X., Zheng Y., Zhang X. Preparation of graphene intercalated magnesium silicate for enhancing the thermal stability and thermal conductivity of ethylene-vinyl acetate copolymer. Polymer. 193 (2020) 122332.

[11] Hull T.R., Quinn R.E., Areri I.G. Combustion toxicity of fire retarded EVA. Poly. Deg. Stab. 77 (2002) 235–242.

[12] Fontaine G., Bourbigot S., Duquesne S. Neutralized flame retardant phosphorus agent: facile synthesis, reaction to fire in PP and synergy with zinc borate. Poly. Deg. Stab. 93 (2008) 68–76.

[13] Camino G., Costa L., Cortemiglia M.P.L. Overview of fire retardant mechanisms. Poly. Deg. Stab. 33 (1991) 131–154.

[14] Hoffendahl C., Fontaine G., Duquesne S. The fire-retardant mechanism of ethylene vinyl acetate elastomer (EVM) containing aluminium trihydroxide and melamine phosphate. RSC Adv. 4 (2014) 20185–20199.

[15] Alongi J., Pošković M., Frache A. Novel flame retardants containing cyclodextrin nano-sponges and phosphorus compounds to enhance EVA combustion properties. Poly. Deg. Stab. 95 (2010) 2093–2100.

[16] Li Y.M., Deng C., Shi X.H. Simultaneously improved flame retardance and ceramifiable properties of polymer-based composites via the formed crystalline phase at high temperature. ACS Appl. Mate. Inter. 11 (2019) 7459–7471.

[17] Pairat R., Sumeath C., Browning F.H. Precipitation and dissolution of calcium-ATMP precipitates for the inhibition of scale formation in porous media. Langmuir. 13(1997) 1791–1798.

[18] Wang Y., Liu J., Tang S. Theoretical research on self-assembly system of molecularly imprinted polymers formed by melamine and trifluoromethacrylic acid. Stru. Chem. 27 (2016) 897–905.

[19] Chng G.Y.Y., Sun X., Cho S.J. Synthesis and 2D self-assembly at the liquid-solid interface of novel H-bonding linear π-conjugated oligomers terminated by uracil and melamine units. New Jour. Chem. 38 (2014) 2407–2413.

[20] Li C., Wu A., Yu W. Parameterizing starch chain-length distributions for structure-property relations. Carb. Poly. 241 (2020) 116390.

[21] Bakshi P.S., Selvakumar D., Kadirvelu K. Chitosan as an environment friendly biomaterial-a review on recent modifications and applications. Inter. Jour. Biol. Mac. 150 (2020) 1072–1083.

[22] Basak S., Ali S.W. Sodium lignin sulfonate (SLS) and pomegranate rind extracts (PRE) bio-macro-molecule: a novel composition for making fire resistant cellulose polymer. Com. Sci. Tech. (2021) 1–19.

[23] Dessbesell L., Paleologou M., Leitch M. Global lignin supply overview and kraft lignin potential as an alternative for petroleum-based polymers. Rene. Sus. Ener. Rev. 123 (2020) 109768.

[24] Deryło M.A., Goworek J., Pikus S. Characterization of melamine-formaldehyde resins by XPS, SAXS, and sorption techniques. Langmuir, 18 (2002) 7538–7543.

[25] Jiang P., Gu X., Zhang S. Synthesis, characterization, and utilization of a novel phosphorus/nitrogen-containing flame retardant. Indus. Eng. Chem. Res. 54 (2015) 2974–2982.

[26] Huang W., Huang J., Yu B. Facile preparation of phosphorus containing hyperbranched polysiloxane grafted graphene oxide hybrid toward simultaneously

enhanced flame retardancy and smoke suppression of thermoplastic polyurethane nanocomposites. Composites Part A: App. Sci. Manu. 150 (2021) 106614.

[27] Xu Z., Chu Z., Yan L. Effect of chicken eggshell on the flame-retardant and smoke suppression properties of an epoxy-based traditional APP-PER-MEL system. Poly. Com. 40 (2019) 2712–2723.

[28] Sundström B. The development of a European fire classification system for building products-test methods and mathematical modelling. Lund University, 2007.

[29] Zanetti M., Camino G., Canavese D. Fire-retardant halogen-antimony-clay synergism in polypropylene layered silicate nanocomposites. Chem. Mate. 14 (2002) 189–193.

[30] Hoffendahl C., Duquesne S., Fontaine G., *et al*. Decomposition mechanism of fire retarded ethylene vinyl acetate elastomer (EVA) containing aluminum trihydroxide and melamine. Poly. Deg. Sta. 113 (2015) 168–179.

[31] Girardin B., Fontaine G., Duquesne S. Measurement of kinetics and thermodynamics of the thermal degradation for flame retarded materials: Application to EVA/ATH/NC. Jour. Ana. Appl. Pyro. 124 (2017) 130–148.

[32] Girardin B., Fontaine G., Duquesne S. Characterization of thermo-physical properties of EVA/ATH: application to gasification experiments and pyrolysis modeling. Mate. 8 (2015) 7837–7863.

[33] Zhou S., Yang Y., Zhu Z. Preparation of a halogen-free flame retardant and its effect on the poly (L-lactic acid) as the flame retardant material. Polymer. 229 (2021) 124027.

[34] Wang Q.Z., Liu C., Xu Y.J. Highly efficient flame retardation of polyester fabrics via novel DOPO-modified sol-gel coatings. Polymer. 226 (2021) 123761.

[35] B. Schartel, T.R. Hull. Development of fire-retarded materials-interpretation of cone calorimeter data, Fir. Mate. 31 (2007) 327–354.

[36] Yang S., Huo S., Wang J. A highly fire-safe and smoke-suppressive single-component epoxy resin with switchable curing temperature and rapid curing rate. Comp. Part B: Engi. 207 (2021) 108601.

[37] Sai T., Ran S., Guo Z. Transparent, highly thermostable and flame retardant polycarbonate enabled by rod-like phosphorous-containing metal complex aggregates. Chem. Engi. Jour. 409 (2021) 128223.

[38] Zhang Y., Jing J., Liu T. A molecularly engineered bioderived polyphosphate for enhanced flame retardant, UV-blocking and mechanical properties of poly (lactic acid). Chem. Eng. Jour. 411 (2021) 128493.

[39] H. Xie, X. Lai, H. Li, X. Zeng. Remarkably-improving the fire-safety of polypropylene by synergism of functionalized ZrP nanosheet and N-alkoxy hindered amine. Appl. Clay. Sci. 166 (2018) 61–73.

[40] Xie H., Lai X., Li H. Synthesis of a novel macromolecular charring agent with free-radical quenching capability and its synergism in flame retardant polypropylene. Poly. Deg. Stab. 130 (2016) 68–77.

[41] Jin X., Sun J., Zhang J.S. Preparation of a novel intumescent flame retardant based on supramolecular interactions and its application in polyamide 11. ACS Appl. Mate. Inter. 9 (2017) 24964–24975.

[42] Shao Z., Deng C., Tan Y. Ammonium polyphosphate chemically-modified with ethanolamine as an efficient intumescent flame retardant for polypropylene. Jour. Mate. Chem. A. 2(2014) 13955–13965.

[43] Yu Y.M., Fu S.Y., Song P.A., Luo X.P. Functionalized lignin by grafting phosphorus-nitrogen improves the thermal stability and flame retardancy of polypropylene. Poly. Deg. Sta. 97 (2012) 541–546.

[44] Liu L.N., Qian M.B., Song P.A. Fabrication of green lignin-based flame retardants for enhancing the thermal and fire retardancy properties of polypropylene/wood composites. ACS Sus. Che. Eng. 4(2016) 2422–2431.

[45] Yang H.T., Yu B., Xu X.D., Bourbigot S., Wang H., Song P.A. Lignin-derived bio-based flame retardants toward high-performance sustainable polymeric materials. Green Chem. 22 (2020) 2129–2161.

[46] Xi X., Pizzi A., Lei H. Environmentally friendly chitosan adhesives for plywood bonding. Inter. Jour. Adhesion. Adhesives. 112 (2022) 103027.

[47] Liu W., Fang C., Wang S. High-performance lignin-containing polyurethane elastomers with dynamic covalent polymer networks. Macro. 52 (2019) 6474–6484.

[48] Liu W., Fang C., Chen F. Strong, reusable, and self-healing lignin-containing polyurea adhesives. Chem. 13 (2020) 4691–470.

[49] Ouyang X., Ke L., Qiu X., Guo Y., Pang Y. Sulfonation of alkali lignin and its potential use in dispersant for cement. Jour. Disp. Sci. Tech. 30 (2009) 1–6.

[50] Li J., Wang W., Zhang S., Gao Q., Zhang W., Li J. Preparation and characterization of lignin demethylated at atmospheric pressure and its application in fact curing biobased phenolic resins. RSC Adv. 6 (2016) 67435–67443.

Graphical Abstract